11 Phase transitions and superconducting photon detectors

O. Bossen, K. Inderbitzin, M. Reibelt, R. Dell'Amore, H. Bartolf, S. Siegrist, L. Gómez, A. Engel and A. Schilling

in collaboration with: Paul Scherrer Institute, University of Bern (K. Krämer), EPF Lausanne (H. Berger), Bhaba Atomic Research Center (G. Ravikumar), Forschungszentrum Karlsruhe (Th. Wolf, H. Küpfer), Tohoku University (N. Toyota), Universität Karlsruhe (K. Il'in), ETH Zürich (J. Karpinksi), Deutsches Zentrum für Luft- und Raumfahrt (H.-W. Hübers), University of Wellington (B. Ruck), Istituto Nazionale di Ricerca Metrologica I.N.RI.M Torino (C. Portesi), FIRST Lab ETH Zürich.

11.1 Physics of superconducting thin-film nanostructures and fast single-photon detectors

Single-photon detectors made from superconducting nanowires are representing a promising new technology: they are extremely fast and have a feasible detection efficiency. These characteristics make them detectors of first choice for a number of quantum correlation experiments or the emerging field of quantum encryption.

The properties of superconducting nanowire single-photon detectors (SNPD) crucially depend on the quality of the unstructured NbN film and the structuring process itself. We have further optimized our mix&match photo- and e-beam lithography process (1) and are now able to produce state-of-the-art single-photon detectors. Starting from a 5 nm thick NbN film (2) with a $T_c \approx 14$ K we have prepared several detectors with different strip widths and filling factors. In Fig. 11.1 a scanning electron microscope (SEM) picture is shown that depicts part of a meander structure with a strip width of only ~ 50 nm.

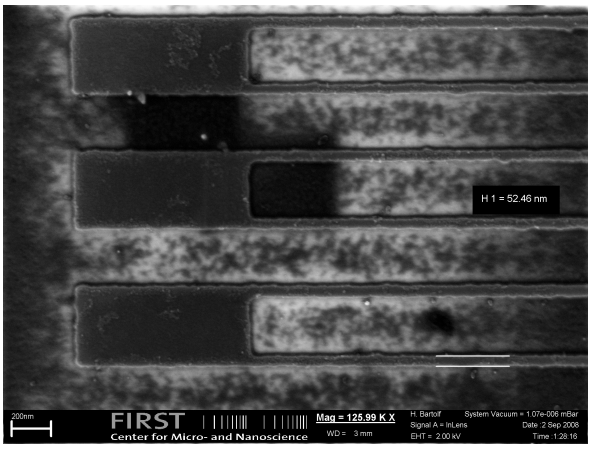

Figure 11.1:
SEM picture of a meander with approximately 50 nm strip width. The filling factor is around 15%.

For all the structures we have measured resistances as a function of temperature and magnetic field from which we could determine normal-state and superconducting properties. This is important to draw any conclusions about the detection mechanism. After the structuring the critical temperatures had dropped slightly to about 12.5 K, but the transitions were still smooth and relatively sharp, indicating very homogeneous meanders. The optical measurements were performed in a ^{4}He-bath cryostat, with the detectors cooled to ≈ 5.5 K. The detectors were biased with a custom-built, battery-powered constant voltage source and shielded from electro-magnetic interferences as much as possible. The continuous spectrum from the light source was passed through a prism monochromator and directed onto the meander through the optical access of the cryostat.

Three of the detectors were characterized in detail. They had different strip widths w and line spacings s, which should be reflected in

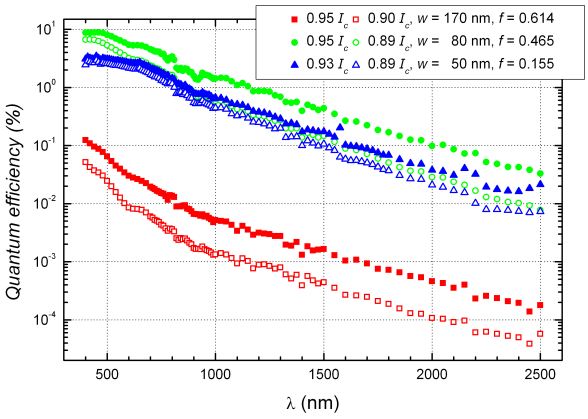

Figure 11.2: Quantum efficiency of three meanders with different strip widths as functions of the incident photon wavelength. Strip widths w and filling factors f are given in the caption.

their detection efficiencies and dark count rates. As an example we show in Fig. 11.2 the quantum efficiency as a function of incident light wavelength for fixed bias currents. The quantum efficiency is defined as the percentage of detected photons from the total flux of photons hitting the meander area per unit time. The data qualitatively fulfil our expectation that narrower meander lines improve the quantum efficiency at longer wavelengths, scaled with the filling factor $f \approx w/(w+s)$. The best achieved quantum efficiency of about 9% is in line with comparable state-of-the-art detectors (see, e.g., Ref. (3)) and further indicates the good homogeneity of the structures. The meander with a strip width of 50 nm reaches a quantum efficiency of roughly 3% (despite having a filling factor of only 0.155), and is one of the world-wide narrowest detectors produced so far.

[1] H. Bartolf, A. Engel, L. Gómez, and A. Schilling, Raith application note, Physics Institute of the University of Zurich, Switzerland (2008).

[2] K. Il'in et al., J. Low Temp. Phys., **151**, (2008) 585.

[3] C. Zinoni et al., Appl. Phys. Lett., **91**, (2007) 031106.

11.2 Search for melting of the flux line lattice in Nb_3Sn and V_3Si

Thermodynamic manifestations for the occurrence of a first order phase transition (FOT) of the vortex system in the mixed state of type II superconductors are well documented for the high-temperature superconductors $YBa_2Cu_3O_7$ and $Bi_2Sr_2CaCu_2O_8$, where it has been interpreted as a melting-like transition of the vortex lattice. Based on general arguments, such a first-order phase transition ought to be seen not only in high-T_c but also in conventional low-T_c superconductors, although it is expected to occur much closer to the upper-critical field H_{c2} (1) – (3).

There are indeed some experimental indications for the occurrence of such a transition very near $H_{c2}(T)$ of certain low-T_c superconductors (2) – (6). Any well developed, sharp first-order like peaks in the specific heat that are comparable to those observed in $YBa_2Cu_3O_7$ are absent in the published data, although very recently Lortz *et al.* interpreted their thermodynamic data on Nb_3Sn in terms of a FLL melting transition (5; 7).

It has been shown that a small ac magnetic field can help the vortices to reach equilibrium in the presence of flux pinning (8; 9). According to theoretical studies on equilibration processes with the help of a small ac field (9), the shaking frequency f should not play any role, but the shaking-field amplitude h_{ac} should be sufficiently large because it is related to the critical sheet current J_c (the current density integrated over the thickness d of the sample) and should fulfill the relation $h_{ac} > J_c/2$. We used an improved version of a low-temperature differential-thermal analysis (DTA) method (10; 11) in combination with an ac shaking magnetic field to measure the specific-heat of Nb_3Sn and V_3Si, and we compared the results with corresponding ac susceptibility and dc magnetization data.

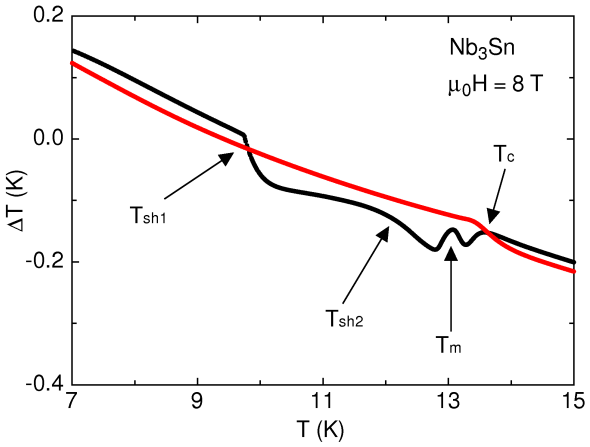

Figure 11.3: Temperature difference ΔT between the two thermometers of our DTA setup for the Nb_3Sn sample in $\mu_0 H = 8$ T. Red curve: Data without ac shaking field. Black curve: Data with an applied ac shaking field ($f = 5$ Hz and $h_{ac} = 0.5$ mT) oriented perpendicular to the main dc field.

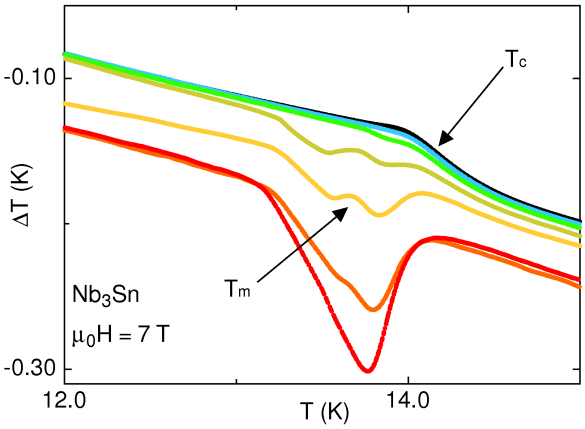

Figure 11.4: DTA-temperature difference for Nb_3Sn in $\mu_0 H = 7$ T and constant frequency $f = 5$ Hz for different shaking field amplitudes h_{ac}, varying form 0 up to ≈ 0.7 mT.

Figure 11.3 shows representative data measured in $\mu_0 H = 8$ T on the same Nb_3Sn crystal as used by Lortz *et al.* in previous studies (5; 7). The figure shows the temperature difference ΔT between the two thermometers of our DTA setup which is related to the specific heat. The red curve shows corresponding data with no ac shaking field, while the black curve shows a measurement with an ac shaking magnetic field oriented perpendicular to the main dc field ($f = 5$ Hz, $h_{ac} \approx 0.5$ mT). The data with vortex shaking exhibit 3 main new features as compared to the data without shaking. At $T_{\rm sh1}$, a self heating process sets in that is likely caused by vortex motion, driven by the ac shaking field which is strong enough to overcome the pinning of the vortices at this temperature. At $T_{\rm sh2}$ a second, additional self heating process seems to set in. Within this second self heating region (at T_m), a bump-like feature occurs for some shaking parameters, superimposed to the self-heating effect. This bump-like feature is reminiscent to a signature of a first order phase transition and may indicate the melting of the vortex lattice, although the transition is rather broad and the latent heat associated with the transition is unusually high. Fig. 11.4 shows the evolution of this self-heating region for different shaking amplitudes. As expected, the self heating increases with increasing shaking amplitude. Interestingly, the bump-like feature at T_m first increases with increasing shaking amplitude, but then decreases for higher amplitudes h_{ac}.

In order to clarify the origin of the observed features, we investigated the same Nb_3Sn crystal also by measuring its ac susceptibility $\chi(T)$. To compare these data with our DTA measurements we chose a comparable frequency ($f = 10$ Hz) and shaking amplitudes. Fig. 11.5 shows one of these measurements for $h_{ac} = 1$ mT (down and up directions are drawn in black and red, respectively). Besides a feature that is usually interpreted as the manifestation of the "peak effect" in the literature (T_p in Fig. 11.5), a shoulder-like feature appears at a $T_m < T_p$, above which the observed hysteresis vanishes as one would expect if a vortex lattice melting transition occurs at T_m.

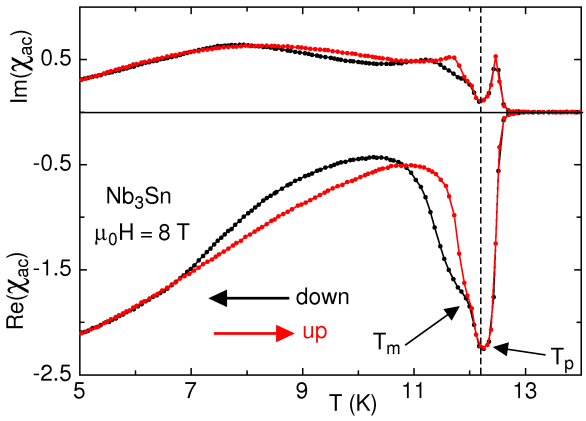

Figure 11.5: Real and imaginary part of the ac susceptibility for Nb_3Sn in $\mu_0 H = 8$ T with $f = 10$ Hz and $h_{ac} = 1$ mT.

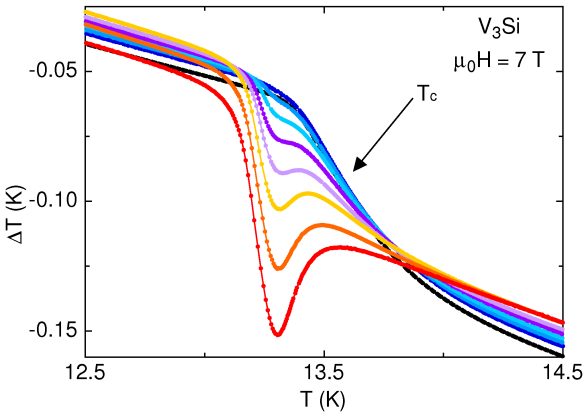

Figure 11.6: DTA-temperature difference for a V_3Si sample in $\mu_0 H = 7$ T and constant frequency $f = 5$ Hz for different shaking field amplitudes h_{ac}, varying form 0 up to ≈ 0.7 mT.

We performed similar DTA measurements on a V_3Si crystal that shares the same cubic "β-tungsten (A-15)" structure with Nb_3Sn. Fig. 11.6 shows a series of DTA measurements at fixed magnetic field $\mu_0 H = 7$ T, fixed ac shaking field frequency $f = 5$ Hz and different amplitudes h_{ac}. The ac shaking field causes again a self heating effect, but with no bump-like feature superimposed as observed in Nb_3Sn. Corresponding magnetic-susceptibility measurements on V_3Si (data not shown) also do not show any related shoulder-like feature below T_p either. We tentatively explain this different behavior of V_3Si with the stronger vortex pinning than in Nb_3Sn that manifests itself in a larger magnetic peak effect, thereby suppressing the melting transition at T_m.

[1] G. P. Mikitik and E. H. Brandt, Phys. Rev. B, **64**, (2001) 184514.

[2] V. A. Marchenko and A. V. Nikulov, JETP Letters, **34**, (1981) 17.

[3] E. Brézin, D. R. Nelson, and A. Thiaville, Phys. Rev. B, **31**, (1985) 7124.

[4] G. Ravikumar and H. Küpfer, Phys. Rev. B, **72**, (2005) 144530.

[5] R. Lortz et al., Phys. Rev. B, **75**, (2007) 094503.

[6] A. Bianchi et al., Phys. Rev. Lett., **91**, (2003) 187004.

[7] R. Lortz et al., Phys. Rev. B, **74**, (2006) 104502.

[8] M. Willemin et al., Phys. Rev. B, **58**, (1998) R5940.

[9] E. H. Brandt and G. P. Mikitik, Phys. Rev. Lett, **89**, (2002) 027002.

[10] A. Schilling and M. Reibelt, Rev. Sci. Instrum., **78**, (2007) 033904.

[11] M. Reibelt et al., Physica C, **468**, (2008) 2254.

11.3 Intrinsic instability of Bose-Einstein condensates in magnetic insulators

Quantum spin systems in solids have become a subject of intense research, both theoretically and experimentally. A number of such systems show magnetic-field induced phase transitions at zero temperature that have been interpreted as a Bose-Einstein condensation (BEC) of magnetic bosonic quasiparticles. In axially symmetric dimerized spin-1/2 systems, one expects a condensation of

triplet bosonic excitations ("triplons") above a certain critical field H_c where the energy difference between the ground-state singlet and the lowest excited triplet states vanishes due to the Zeeman splitting. Despite the large number of experimental papers on the occurrence of BEC in magnetic insulators there is no direct proof for the existence of such a condensate, i.e., the demonstration of macroscopic phase coherence or even superfluidity of corresponding spin currents. To the best of our knowledge, the only attempt to find a direct experimental evidence for such a macroscopic quantum state in $TlCuCl_3$ has been undertaken in our group but has not shown any sign for such a coherent quantum state in $\mu_0 H = 9$ T on a time scale larger than 0.5 μs (see previous annual reports). The notorious lack of experimental evidence supporting the existence of a long-lived phase coherent condensate in any real material is, from an experimental point of view, highly unsatisfactory.

To further analyze this problem we have used a standard functional method to describe dilute Bose gases in the classical limit at $T = 0$ that provides an extremal condition for the potential energy u of the condensate per dimer in such systems (1). Including a perturbation term $\gamma(\Psi\Psi + \Psi^*\Psi^*)$ with $\gamma > 0$ that explicitly violates axial symmetry (2; 3) we obtain the condition

$$\begin{aligned} u(\Psi) &= -\mu\Psi^*\Psi + \gamma\left(\Psi\Psi + \Psi^*\Psi^*\right) + \frac{\nu_0}{2}\left(\Psi^*\Psi\right)^2 \\ &= min.\,, \end{aligned}$$

where $\Psi(r,t)$ is the complex scalar field describing the BEC condensate, $\mu(H) = g\mu_B\mu_0(H - H_c)$ is the chemical potential with the Landé g-factor, and ν_0 is the two-particle interaction potential (4).

An important consequence of a violated axial symmetry is that the potential energy at H_c for the optimum $\Psi_0(r) = |\Psi_0|\, e^{i\phi}$ is smaller for $\gamma > 0$ (by $\Delta u = 2\gamma^2/\nu_0$) than for an axially symmetric system with $\gamma = 0$ (see Figs. 11.7 and 11.8), and the corresponding phase $\phi = \pm\pi/2$ is fixed. This means that an originally axially

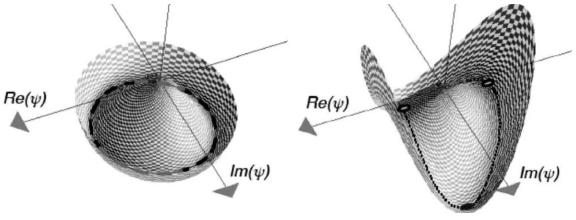

Figure 11.7: (a) Potential energy $u(\Psi)$ for axial symmetry ($\gamma = 0$). The minima are located on a circle with arbitrary phase ϕ (dashed line). (b) $u(\Psi)$ for violated axial symmetry ($\gamma > 0$). The potential energy at the isolated minima (filled circles) is lower than that of an axially symmetric system.

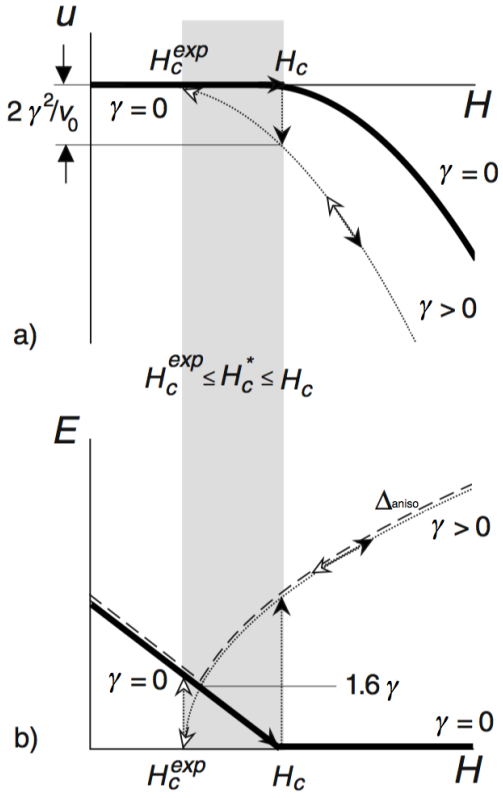

Figure 11.8: (a) Potential energy and (b) energy-level scheme of the lowest triplon branch of an axially symmetric system ($\gamma = 0$, solid lines) and of a system that shows a spontaneous violation of axial symmetry ($\gamma > 0$) at a field H_c^* with $H_c^* \le H_c$ (dashed line). Arrows indicate the maximum possible hysteresis for increasing and decreasing magnetic field, respectively (shaded area)

symmetric system ($\gamma = 0$) tends to spontaneously distort ($\gamma > 0$) as soon as the BEC is formed at H_c as long as the total energy, including the crystal-lattice contribution, is lowered along with this distortion. As the potential energy may jump discontinuously at a $H_c^* < H_c$ (see Fig. 11.8a), the transition is probably of weakly-first order. Moreover, the resulting state above H_c^* cannot be regarded as a superfluid because the spin-supercurrent velocity $v_s = \hbar m^* \nabla \phi$ is strictly zero.

Our results easily explain why no experiment has ever detected any superfluid-like response in any magnetic insulator. It also accounts for numerous observations of first-order like effects at the critical fields of $TlCuCl_3$ (5; 6) and of the spin-1 system $NiCl_2$-4SC$(NH_2)_2$ (7). These arguments are so general that they should be applicable to all insulating spin systems that are supposed to show a Bose-Einstein condensation of magnetic bosonic quasiparticles, and we expect that all magnetic BEC systems in insulating spin systems are intrinsically unstable toward a spontaneous anisotropic distortion perpendicular to the external magnetic field.

[1] J. O. Andresen, Rev. Mod. Phys., **76**, (2004) 599.

[2] I. Affleck, Phys. Rev. B, **43**, (1991) 3215.

[3] J. Sirker, A. Weisse and O. P. Sushkov, J. Phys. Soc. Jpn., **74**, (2005) 129.

[4] R. DellŠAmore, A. Schilling and K. Krämer, Phys. Rev. B, **79**, (2009) 014438.

[5] O. Vyaselev et al., Phys. Rev. Lett., **92**, (2004) 207202.

[6] E. Ya. Sherman et al., Phys. Rev. Lett., **91**, (2003) 057201.

[7] V. S. Zapf et al., Phys. Rev. Lett., **96** (2006) 077204.